JOURNAL OF COMPUTATIONAL PHYSICS 113, 268–278 (1994)

Finite Element Method for Conservation Equations in Electrical Gas Discharge Areas

M. YOUSFI, A. POINSIGNON, AND A. HAMANI

Université Paul Sabatier, URA du CNRS n° 277, CPAT, 118, Route de Narbonne, 31 062 Toulouse cedex, France

Received August 9, 1993

A powerful finite element method for numerical solution of hydrodynamic conservation equations of electrons and ions, including drift, diffusion, and source terms, is proposed and applied in the area of electrical gas discharges dominated by space charge effects and having steep variation of charge carrier densities. This numerical method, having a quite good conservative property and valid also for non-uniform mesh case, is able to take properly into account the possible discontinuities in space and/or time variation of electron and ion densities. Comparisons with an implicit finite difference scheme are first undertaken in the case of a standard problem of propagation of rectangular and Gaussian initial waves without source term and with or without diffusion. Then, in the case of real discharges between two plane parallel electrodes, hydrodynamic equations for charge carrier conservation coupled to Poisson equation have been solved. This has been undertaken to show the ability of the present numerical method to treat the classical discharges dominated by space charge effects such as the cathodic region of usual glow discharge in Ar and the propagation of ionizing waves in high pressure N_2 discharge under overvoltage stress.

1. INTRODUCTION

In this paper, a finite element method has been applied to the numerical solution of hydrodynamic conservation equations for charge carriers (electrons and ions) evolving in non-thermal cold plasmas created by electrical gas discharges. As is known, these plasmas are characterized by a relatively low ionization degree ($n_e/N < 10^{-4}$, n_e and N being electron and background gas densities) and an electron temperature generally much higher than the temperature of neutral gas which remains practically at the ambient temperature during discharge evolution. In fact, the present numerical method concerns, more particularly, gas discharges in which space charge effects can lead to a strongly non-uniform electric field and very steep density gradients, such as the cathode region of usual glow discharges or plasma generated by ionizing waves under overvoltage stress as in corona discharges.

In these gas discharge areas, the most used numerical algorithms, in the literature, in approximately the last three decades, can be roughly divided into three classes: the hybrid method of characteristics, the FCT (flux corrected transport) algorithms, and the implicit finite difference scheme.

In the framework of this paper, there are no detailed descriptions of, or exhaustive references to, these different numerical algorithms already successfully applied—with their advantages and disadvantages—for the solution of continuity equations for the study of space charge dominated transport in gases. However, the interested reader can refer, for example, to Davies *et al.* [1] concerning the hybrid method of characteristics developed mainly to trace the space and time ionization growth under important space charge effects. This method, where continuity equations for electrons and ions are integrated along the characteristic curves, has real advantages (easily understandable physically and second-order accuracy) and has been then used by several authors [2]. However, due to, in particular, its iterative nature which involves rather long computational times, this method has been progressively replaced by alternative method beginning around 1980. Among the numerous finite difference schemes which have been successfully used in the literature in the field of gas discharges (as, e.g., the explicit relaxation method of Lowke and Davies [3]), the flux corrected transport (FCT) scheme is today probably the one most used. This FCT numerical scheme, which is analyzed by Morrow [4] and compared to Euler, Runge–Kutta, Lax–Wendroff schemes, and also to the characteristic method, has been developed, first, in the area of fluid dynamics by Boris and Book [5] and Zalesak [6] for the propagation of steep shock waves. FCT schemes, under different forms (non-uniform meshes, implicit formulation, in 1D and 2D geometry, etc.) have been used then for the numerical computation of electrical breakdown in non-uniform fields by several authors [7]. However, even though the Courant–Friedrichs–Lewy condition (concerning time step Δt and grid space Δz for particle velocity W) is restricted [4] to $\Delta t < \Delta z/2W$ instead

0021-9991/94 $6.00

of $\Delta t < \Delta z/W$ for the usual explicit finite difference scheme, FCT algorithms, particularly in the case of 2D geometry, are not powerful enough to be really attractive from a computational time point of view. Then, another finite difference method (implicit scheme with exponential solution), initially developed in semi-conductor device simulation [8], has been adapted to charged particle transport in the case of dc and rf glow discharges by Boeuf [9] for 1D and also 2D geometry. This scheme is, in principle, not subject to a severe limitation for choice of Δt time step (due to its implicit formulation) and is able to treat (due to its exponential solution) transport of charged particles in the cases where predominate drift term as well as diffusion term and also in the case of relatively high current density (e.g., as in highly abnormal glow discharges). However, the change from 1D to 2D geometry is not a straightforward transformation.

In fact, in comparison to most of the previous numerical schemes, finite element method (proposed in this paper for solution of continuity equations of electrons and ions) presents a major drawback linked to its programming complexity especially in the case, where the solution has discontinuity along the z and/or time axis. However, despite this difficulty, finite element methods can be considered attractive enough, from the authors' point of view, regarding its numerous advantages: boundaries are correctly treated, only density values are needed as boundary conditions and not their space derivatives, solution remains positive without specifying any numerical constraint, choices of Δt time step and Δz space grid are less restrictive, numerical scheme is straightforwardly transformed from 1D to 2D or 3D geometry, and discontinuity on solution can be properly taken into account.

Furthermore, as is known, finite element schemes have already been successfully applied for a long time to several areas such as, for example, Boltzmann equation for electrons in weakly ionized gases [10], or Boltzmann equation for neutron tranport theory [11], or fluid equations in semi-conductor device simulation [12], etc. In the latter area, Barnes and Lomax [12] have already shown the ability of finite element methods to solve continuity equations for electrons and holes coupled to Poisson equation which are quite similar to equations of electrons and ions in gases. Therefore, these similitudes to semiconductor area and also to neutron transport [11] and electron transport [10] areas, have been used in this paper as a source of suggestions to apply a specific finite element method for solution of charge carrier conservation equations in gas discharge field. In that field, in the authors' knowledge, such a numerical scheme has not yet been adapted in the literature since usual schemes, as outlined previously, are based rather on finite difference algorithms.

So, in the framework of this paper, a specific finite element scheme is described in the case of typical time dependent and non-linear hydrodynamic equation for charge carriers including convective, diffusion and source terms for 1D Cartesian geometry. This coordinate frame is chosen in order to illustrate the numerical scheme (see Section 2). This rather complex method, already used in the neutron transport area [13] and also for electron transport in weakly ionized gases [10], is a discontinuous finite element method where an a priori continuity between two consecutive grids is not assumed. However, it can easily be reduced to a simpler scheme (continuous finite element method) when there is no discontinuity in the density variation. In Section 3, some results are first given in model gas discharge (i.e., without source term and with or without diffusion term) in order to check the validity and the powerfulness of this numerical scheme, for instance, in the case of the propagation of test functions such as rectangular or Gaussian waves. Comparisons are also undertaken with an implicit finite difference scheme. Then, some results are given in the case of real discharges corresponding to cathodic region of Ar glow discharge and also for propagation of ionizing wave in high pressure N_2 discharges under overvoltages stress. The aim is to show the ability of the finite element method to correctly describe the main features of charge carrier transport in these discharges dominated by highly non-uniform electric fields due to space charge effects which are taken into account, as usual, by coupling Poisson equation to hydrodynamic conservation equation of electrons and ions.

2. NUMERICAL METHODS OF CALCULATION

2.1. *Hydrodynamic Equations for Charge Carriers*

The space and time evolution of hydrodynamic equations for charge carriers (or continuity equations) can be written in the case of 1D Cartesian geometry as

$$\frac{\partial \rho^e}{\partial t} + \frac{\partial j_z^e}{\partial z} = \rho^e(\nu_i - \nu_a) \tag{1a}$$

$$\frac{\partial \rho^+}{\partial t} + \frac{\partial j_z^+}{\partial z} = \rho^e \nu_i \tag{1b}$$

$$\frac{\partial \rho^-}{\partial t} + \frac{\partial j_z^-}{\partial z} = \rho^e \nu_a, \tag{1c}$$

where ρ^e, ρ^+, and ρ^- are electron, positive ion, and negative ion charge densities; j_z^e, j_z^+, j_z^- are their respective current densities along the z axis. Axial j_z component of current densities for any charged particles (electron, positive ion, or negative ion) has the following form:

$$j_z = \rho W_z - D_z \frac{\partial \rho}{\partial z}. \tag{2}$$

In Eq. (1), ν_i and ν_a represent ionization and attachment frequencies due to electron–molecule impact (for the sake of simplicity, ions are assumed to be produced only by electron–molecule collision). While in Eq. (2), W_z can be the axial electron, positive ion, or negative ion drift velocities (W_z^e, W_z^+, or W_z^-) due to electrid field action on charge carriers and D_z, the axial diffusion coefficients of the corresponding particles (D_z^e, D_z^+, or D_z^-). In fact, ion diffusion coefficients are often neglected in the literature in Eq. (2). Such an approximation, which can be correct on a short time scale, becomes more questionable on a longer time scale where ion drift and diffusion have a more significant influence.

Furthermore, due to the important space charge effect in the discharge of our interest, Eqs. (1) and (2) are strongly coupled to Poisson equation for potential V (or for axial electric field E_z) which, in 1D Cartesian geometry, has the form

$$\frac{\partial^2 V}{\partial z^2} = -\frac{\partial E_z}{\partial z} = -\frac{1}{\varepsilon_0}(\rho^+ + \rho^e + \rho^-), \tag{3}$$

where ε_0 denotes the dielectric constant.

2.2. *Numerical Schemes*

The general form of conservation equations of charged particles to be solved is obtained by substituting Eq. (2) in Eq. (1),

$$\frac{\partial n(z,t)}{\partial t} + \frac{\partial n W_z(z,t)}{\partial z} - \frac{\partial}{\partial z}\left\{D_z(z,t)\frac{\partial}{\partial z}n(z,t)\right\} = S(z,t) \tag{4}$$

with known initial ($n(z, t=0)$) and boundary ($n(z=z_{\min}, t)$ or $n(z=z_{\max}, t)$) conditions.

In Eq. (4), $n(z, t)$ can be electron, positive ion, or negative ion density, and $S(z, t)$, $W_z(z, t)$, and $D_z(z, t)$ are source term, drift velocity, and diffusion coefficient of the corresponding particles. In fact, Eq. (4) is generally solved using the local electric field approximation in which the macroscopic coefficients (W_z, D_z, ν_i, and ν_a) depend on space and time via the electric field $E_z(z, t)$ such as, for example, $W_z(E_z(z,t))$, $D_z(E_z(z,t))$. In the framework of this paper, the well-known non-equilibrium effects (see, e.g., [14]), not taken into account by local electric field approximation, are not discussed. However, it must be noted that Eqs. (4), coupled to Poisson equation (3) and using local electric field approximation (i.e., fluid model), are, in principle, not sufficient to give realistic gas discharge parameters (electron and ion densities, sheath thickness, ...) in the case of, for example, abnormal glow discharge. Indeed, in that case, local field approximation is no more valid since ionization processes are overestimated in the sheath (cathode region) and underestimated in the negative glow (see, e.g., [9, 14]). In order to obtain more realistic discharge parameters, it is necessary to avoid local field approximation by coupling to a fluid model, for instance, the Boltzmann equation or Monte Carlo simulation, which are able to take into account correctly the non-equilibrium effects on transport coefficients. But, in any case, numerical solution of hydrodynamic equations (4) are still necessary, and an optimum numerical scheme reducing, for example, time computing or numerical diffusion, is always suitable. This is one of the reasons for which the following numerical scheme is described hereafter.

It has been previously noted that Eq. (4) (which is a highly non-linear second-order partial differential equation and strongly coupled to Poisson equation (3)) can be numerically solved using a classical finite difference scheme based on discretization of the different differential operators $\partial/\partial t$ and $\partial/\partial z$. Such a direct method, called strong formulation, necessitates, in principle, further conditions on space and time derivatives of density $n(z, t)$. Such conditions are not always known and not so easy—in certain cases—to introduce in the numerical scheme. Another way to solve Eq. (4) is to use a less restrictive formulation (weak formulation) which is less demanding concerning conditions on time and space derivatives of density. The weak formulation consists of replacing, as in weighted residual method, Eq. (4) by an integral equation:

$$\int dz \int dt\, \phi \left(\frac{\partial n(z,t)}{\partial t} + \frac{\partial n W_z(z,t)}{\partial z} - \frac{\partial}{\partial z}\left[D_z(z,t)\frac{\partial}{\partial z}n(z,t)\right]\right) = \int dz \int dt\, \phi S(z,t), \tag{5}$$

where ϕ is a known test function. The meaning of this test function ϕ can be found in the abundant literature devoted to finite element methods for partial differential equations (see, e.g., Zienkiewicz [15]). However, it is to be noted that if $n(z, t)$ satisfies Eq. (5) whatever the test function ϕ, then Eqs. (4) and (5) are identical or, in other words, Eqs. (4) and (5) have the same solution. But, if $n(z, t)$ satisfies Eq. (5) for a large enough set of independent test functions, then $n(z, t)$ can be considered as an approximate solution of

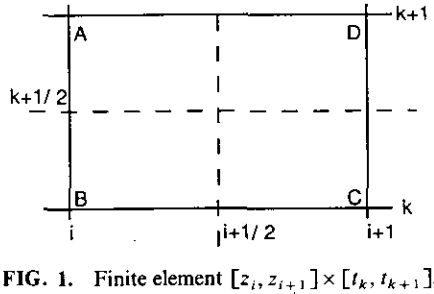

FIG. 1. Finite element $[z_i, z_{i+1}] \times [t_k, t_{k+1}]$.

Eq. (4) with an acceptable degree of confidence. This is why the weak formulation (i.e., integral equation (5)) can be chosen for the numerical solution of hydrodynamic equations of charge carriers.

To do that, it is necessary first to define the limits of space z and time t domains and to discretize the corresponding domains respectively in nz and nt intervals,

$$z = \{z_{\min}, z_{\max}\}$$
$$= \{z_0 = z_{\min}, z_1, z_2, ..., z_i, z_{i+1}, ..., z_{nz} = z_{\max}\},$$
$$t = \{t_{\min}, t_{\max}\}$$
$$= \{t_0 = t_{\min}, t_1, t_2, ..., t_k, t_{k+1}, ..., t_{nt} = t_{\max}\},$$

where $\Delta z_{i+1/2}$ $(= z_{i+1} - z_i)$, the space step, and $\Delta t_{k+1/2}$ $(= t_{k+1} - t_k)$, the time step, are not necessarily regular. In this paper, each finite element $[z_i, z_{i+1}] \times [t_k, t_{k+1}]$ is chosen as a rectangular grid (see Fig. 1).

Then in each finite element, Eq. (4) is multiplied by the known test function ϕ and integrated over dz and dt. As, $n(z, t)$ is assumed to be a linear function of variables z and t inside each finite element, i.e.,

$$n(z, t) = az + bt + c, \tag{6}$$

test functions ϕ are chosen, as in Chauvet's work [13], linear in $[z, t]$ space:

$$\phi_j = z^l t^m \qquad \text{with} \quad l = 0 \text{ or } 1 \text{ and } m = 0 \text{ or } 1 \text{ (see Table 1).}$$

Furthermore, it is important to note that the direction of integration (i.e., for a given time step $\Delta t_{k+1/2}$, the displacement along the z axis from a finite element to the adjoining one) corresponds to the real direction of particle displacement in the gas discharge (i.e., from cathode to anode for electrons and negative ions and from anode to cathode for positive ions), while the direction of integration along the time axis is always along the direction of time evolution. For these reasons, Chauvet [13] has defined (as in an upwind differencing method) the "lighted sides" (or the upstream sides) of each finite element $[z_i, z_{i+1}] \times [t_k, t_{k+1}]$ which are the sides of entrance in the grid (i.e., sides AB and BC shown in Fig. 1 in the case of negative particles and sides CD and BC for positive ions). So, in the case where $n(z, t)$ has discontinuities along the z and/or t axis, the discontinuity notion must intervene in the definition of $n(z, t)$ itself, which is not the same inside the elementary grid and in the lighted sides; this yields

$$n(z, t) = n_{\text{in}}(z, t) + \delta_{i,k}\{n_{\text{out}}(z, t) - n_{\text{in}}(z, t)\}, \tag{7}$$

where $n_{\text{out}}(z, t)$ and $n_{\text{in}}(z, t)$ are, respectively, the density outside and inside the elementary grid $[z_i, z_{i+1}] \times [t_k, t_{k+1}]$; $\delta_{i,k} = 1$ in the lighted sides and $\delta_{i,k} = 0$ elsewhere. As the density $n_{\text{in}}(z, t)$ is assumed varying linearly inside the elementary grid, then $n_{\text{in}}(z, t)$ can be expressed as a function of densities of each grid corner (A, B, C, or D) shown in Fig. 1, following the expression deduced from linear relation (6):

$$n_{\text{in}}(z, t) = \frac{1}{\Delta z_{i+1/2}\, \Delta t_{k+1/2}} \times \{n_A(z_{i+1} - z)(t - t_k) + n_B(z_{i+1} - z)(t_{k+1} - t) + n_C(z - z_i)(t_{k+1} - t) + n_D(z - z_i)(t - t_k)\}. \tag{8}$$

Then, in following relation (9), time and space derivatives of the density $n(z, t)$ ($\partial n/\partial t$ and $\partial n/\partial z$) need to be considered in a distribution sense; these yields

$$\frac{\partial n(z, t)}{\partial t} = \left\{\frac{\partial n_{\text{in}}(z, t)}{\partial t}\right\} - \delta(t - t_k) \times [n_{\text{out}}(z, t_k) - n_{\text{in}}(z, t_k)], \tag{9a}$$

$$\frac{\partial n(z, t)}{\partial z} = \left\{\frac{\partial n_{\text{in}}(z, t)}{\partial z}\right\} + s\delta(z - z_{i+(s+1)/2}) \times [n_{\text{out}}(z_{i+(s+1)/2}, t) - n_{\text{in}}(z_{i+(s+1)/2}, t)], \tag{9b}$$

where $\{\partial n_{\text{in}}(z, t)/\partial t\}$ and $\{\partial n_{\text{in}}(z, t)/\partial z\}$ are time and space derivatives with the classical meaning and δ is the Dirac function: $s = -1$ in side AB, i.e., for electrons and negative ions (particles moving forwards on the z axis); $s = +1$ in side CD, i.e., for positive ions (particles moving backwards on the z axis).

From the previous definitions (9), Eq. (5), for a completely discontinuous density (i.e., along t and z axis), becomes

$$\int_{z_i}^{z_{i+1}} dz \int_{t_k}^{t_{k+1}} dt\, z^l t^m \left(\left\{\frac{\partial n_{\text{in}}(z, t)}{\partial t}\right\} + \left\{\frac{\partial n_{\text{in}} W_z(z, t)}{\partial z}\right\} - \left\{\frac{\partial}{\partial z}\left[D_z(z, t)\frac{\partial}{\partial z} n_{\text{in}}(z, t)\right]\right\}\right) - \int_{z_i}^{z_{i+1}} dz \int_{t_k}^{t_{k+1}} dt\, z^l t^m \delta(t - t_k)(n_{\text{out}}(z, t_k) - n_{\text{in}}(z, t_k))$$

TABLE I

Definition of Test Functions ϕj for the Different Values of l and m

j	l	m	ϕj
1	0	0	1
2	1	0	z
3	0	1	t
4	1	1	zt

$$+s\int_{z_i}^{z_{i+1}} dz \int_{t_k}^{t_{k+1}} dt\, z^l t^m \delta(z - z_{i+(s+1)/2})\, W_z(z, t)$$
$$\times (n_{out}(z_{i+(s+1)/2}, t) - n_{in}(z_{i+(s+1)/2}, t))$$
$$-s\int_{z_i}^{z_{i+1}} dz \int_{t_k}^{t_{k+1}} dt\, z^l t^m \delta(z - z_{i+(s+1)/2})\, D_z(z, t)$$
$$\times \left(\left| \frac{\partial n_{out}(z, t)}{\partial z} \right|_{z = z_{i+(s+1)/2}} - \left| \frac{\partial n_{in}(z, t)}{\partial z} \right|_{z = z_{i+(s+1)/2}} \right)$$
$$= \int_{z_i}^{z_{i+1}} dz \int_{t_k}^{t_{k+1}} dt\, z^l t^m S(z, t). \tag{10}$$

Noting that description of the numerical scheme is devoted to the discontinuous finite element method; knowing that, in the continuous case, all terms including discontinuity (i.e., the Dirac function) must be removed.

Equation (10) is first integrated over dt and dz inside the elementary grid (i.e., without discontinuity terms), by using linear relation (6), this yields the following relation in the case of negative particles:

$$n_A \left\{ \overline{t^m_{k+1/2}}\,\overline{\zeta^{l+1}_{i+1/2}} - \overline{z^l_{i+1/2}}\,\tau^{m+1}_{k+1/2} \times \left[W_{z^{k+1/2}_{i+1/2}} - \frac{D_{z^{k+1/2}_{i+1}}}{\Delta z_{i+1/2}} - \frac{D_{z^{k+1/2}_i}}{\Delta z_{i-1/2}} \right] \right\}$$
$$+ n_B \left\{ -\overline{t^m_{k+1/2}}\,\overline{\zeta^{l+1}_{i+1/2}} - \overline{z^l_{i+1/2}}\,\overline{\tau^{m+1}_{k+1/2}} \times \left[W_{z^{k+1/2}_{i+1/2}} - \frac{D_{z^{k+1/2}_{i+1}}}{\Delta z_{i+1/2}} - \frac{D_{z^{k+1/2}_i}}{\Delta z_{i-1/2}} \right] \right\}$$
$$+ n_C \left\{ -\overline{t^m_{k+1/2}}\,\zeta^{l+1}_{i+1/2} + \overline{z^l_{i+1/2}}\,\overline{\tau^{m+1}_{k+1/2}} \times \left[W_{z^{k+1/2}_{i+1/2}} - \frac{D_{z^{k+1/2}_{i+1}}}{\Delta z_{i+1/2}} \right] \right\}$$
$$+ n_D \left\{ -\overline{t^m_{k+1/2}}\,\zeta^{l+1}_{i+1/2} + \overline{z^l_{i+1/2}}\,\tau^{m+1}_{k+1/2} \times \left[W_{z^{k+1/2}_{i+1/2}} - \frac{D_{z^{k+1/2}_{i+1}}}{\Delta z_{i+1/2}} \right] \right\}$$
$$= t^m_{k+1/2} z^l_{i+1/2} S(z_{i+1/2}, t_{k+1/2}) + \overline{z^l_{i+1/2}}\,\tau^{m+1}_{k+1/2} \frac{D_{z^{k+1/2}_i}}{\Delta z_{i-1/2}} n(z_{i-1}, t_{k+1}) + \overline{z^l_{i+1/2}}\,\overline{\tau^{m+1}_{k+1/2}} \frac{D_{z^{k+1/2}_i}}{\Delta z_{i-1/2}} n(z_{i-1}, t_k). \tag{11}$$

Coefficients $\overline{z^l_{i+1/2}}$, $\overline{t^m_{k+1/2}}$, $\zeta^{l+1}_{i+1/2}$, $\overline{\zeta^{l+1}_{i+1/2}}$, $\tau^{m+1}_{k+1/2}$, and $\overline{\tau^{m+1}_{k+1/2}}$ are defined in the Appendix and $D_{z^{k+1/2}_i}$, $D_{z^{k+1/2}_{i+1}}$ are diffusion coefficients at $t_{k+1/2}$, and z_i and z_{i+1}, respectively, and $W_{z^{k+1/2}_{i+1/2}}$ drift velocity at $t_{k+1/2}$ and $z_{i+1/2}$.

Then discontinuous terms of Eq. (10) are integrated over dt and dz by using definitions shown in Fig. 2 for densities inside and outside each elementary grid. These definitions include the case where, for the same grid point (e.g., point B having coordinates z_i, t_k), densities inside n_B and outside n_{Bz} can be different due to a possible discontinuity. In fact, for a given finite element, densities inside the grid n_A, n_B, n_C, and n_D are not yet known, and densities outside the grid (i.e., densities n_{Bt}, n_{Ct} and n_{Az}, n_{Bz} in lighted sides BC and AB for negative particles and densities n_{Bt}, n_{Ct}, and n_{Cz}, n_{Dz} in lighted sides BC and CD for positive ions) are already known because these densities are previously calculated in the grids surrounding the working grid $[z_i, z_{i+1}] \times [t_k, t_{k+1}]$. Obviously, for a continuous scheme, densities n_A and n_{Az} or n_B and n_{BZ} or n_B and n_{Bt} are identical (i.e., $n_A = n_{Az}$, $n_B = n_{Bz} = n_{Bt}$).

So, integration over dt and dz of discontinuous terms of Eq. (10), in the case of negative particles (sides AB and BC), gives

$$-t^m_k \left\{ (n_{Bt} - n_B)\,\overline{\zeta^{l+1}_{i+1/2}} + (n_{Ct} - n_C)\,\zeta^{l+1}_{i+1/2} \right\} - z^l_i \left\{ W_{z^{k+1/2}_i} - \frac{D_{z^{k+1/2}_i}}{\Delta z_i} \right\} \times \left\{ (n_{Bz} - n_B)\,\overline{\tau^{m+1}_{k+1/2}} + (n_{Az} - n_A)\,\tau^{m+1}_{k+1/2} \right\} \tag{12}$$

with $\Delta z_i = z_{i+1/2} - z_{i-1/2}$.

Therefore, in each elementary grid, relations (11) and (12) lead to a linear system of four equations and four unknowns (i.e., densities n_A, n_B, n_C, and n_D) obtained for the different values of l and m corresponding to the four possible combinations (or degrees of freedom according to the Chauvet [13] definition) as is shown in Table I. Such a system of four linear equations (given in appendix for negative and positive particles), which is solved with a classical numerical method, gives the sought solutions n_A, n_B, n_C, and n_D in each elementary grid. Obviously, in the

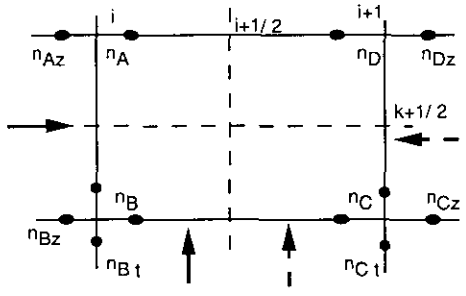

FIG. 2. Finite element $[z_i, z_{i+1}] \times [t_k, t_{k+1}]$ showing schematically densities n_A, n_B, n_C, and n_D inside the grid and densities outside the grid for lighted side BC (n_{Bt}, n_{Ct}), for lighted side AB (n_{Az}, n_{Bz}), and for lighted side CD (n_{Cz}, n_{Dz}) (full arrows show the direction of entrance into the grid in the case for electrons and negative ions and dashed arrows for positive ions).

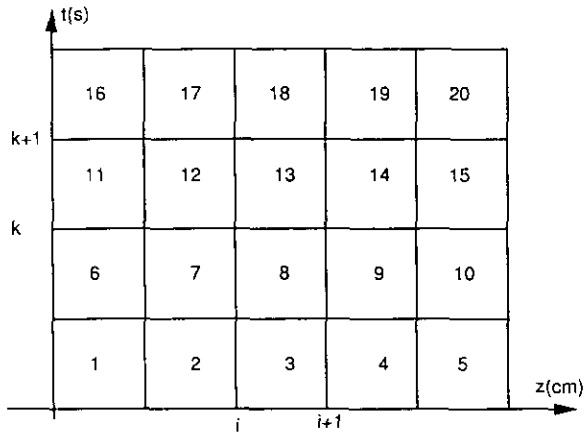

FIG. 3. Direction of integration from one grid to the adjoining one (grid number 1 to grid number 20) in the case of particles moving in forwards direction (negative particles).

case of continuous density, this system reduces to one equation (obtained for $l=0$ and $m=0$) with one unknown which is either n_B for negative particles or n_C for positive particles.

Then, in order to obtain solution in the whole integration domain $[z_{\min}, z_{\max}] \times [t_{\min}, t_{\max}]$, the successive elementary grids are treated one by one along the z axis and then along time axis as is depicted in Fig. 3 (in the case of negative particles), where the direction of integration corresponds to the direction of displacement of particles in the gap discharge (from cathode to anode for electrons and negative ions and from anode to cathode for positive ions). This is why finite element method needs as boundary conditions only the knowledge of density at the cathode for negative particles and density at the anode for positive particle; the knowledge of space derivative of density is not required as in finite difference scheme. This is also the reason for which the finite element scheme is relatively stable and strictly conservative; this means, in absence of reactive processes, density of charged particles is perfectly conserved during the drift and diffusion of particles in a gas discharge, as will be shown in next section.

3. RESULTS

3.1. *Results in Model Discharges*

The finite element scheme previously described is firstly tested on a standard problem in which diffusion and source terms are neglected, i.e.,

$$\frac{\partial n}{\partial t} + \frac{\partial n W_z}{\partial z} = 0. \tag{13}$$

As in Davies's paper [16] in which the performance of several numerical schemes are analyzed (hybrid method of characteristics, FCT, monotonic upstream-centred scheme for conservation law or MUSCL schemes, etc.), Eq. (13) is solved under the following conditions:

— domain of z variation is: $[0, 1]$

— initial density $n(z, t=0)$ is a discontinuous function along z axis:

$$n(z, t=0) = 10 \quad \text{for} \quad 0.05 \leqslant z \leqslant 0.25$$
$$\text{and } n(z, t=0) = 0 \text{ elsewhere}$$

— drift velocity is space dependent: $W_z(z) = 1 + 9 \sin^8 \pi z$

— boundaries are periodic in the sense that any particle leaving the right limit ($z=1$) enters at the left limit ($z=0$) so that after a period $T = \int_0^1 dz/W_z(z)$, solution $n(z, t=T)$ should be identical with initial distribution $n(z, t=0)$.

Figure 4a shows initial rectangular density $n(z, t=0)$ and ideal solutions of Eq. (13) (for $t=0.4T$ and $t=T$) compared to densities calculated from the finite element method. It is easy to observe that, except for $z=0.05$ and $z=0.25$, where $n(z, t=T)$ presents (in comparison) to ideal solution a small disturbance on the top of density, the agreement between ideal and finite element method results is remarkably satisfying. In Fig. 4b, numerical calculations (obtained from a classical implicit finite difference scheme under the same conditions) show non-negligible numerical diffusions enlarging the base of density $n(z, t=T)$ and reducing its top. These numerical diffusions have also the same effect on solution $n(z, t=0.4T)$ where, in particular, the decay of peak height is quite pronounced in comparison with the ideal solution. Such numerical diffusions and peak decay are practically unobserved in the case of finite element method. From these results and also from those given by Davies [16] using several numerical schemes (FCT, hybrid method of characteristic, MUSCL) under the same conditions, it is reasonable to conclude that the present finite element method is able to treat the discontinuity problem in the most satisfying way.

Furthermore, concerning the discontinuity problem, it is to be noted in the cases of real gas discharges that the kind of discontinuity shown in Figs. 4 is not very usual, except for charge carrier densities generated by the ionizing wave in high pressure discharge under overvoltage stress, as is shown in the next section. However, even though densities are very steep in these real discharges, the space density derivative is not really infinite as in the rectangular function test. So, for this reason and also to save computation times, the following finite element method calculations are undertaken without including discontinuity terms shown in Eqs. (A1) and (A2) of the Appendix, except if the density derivative becomes infinite.

A second test function without discontinuity (an initial

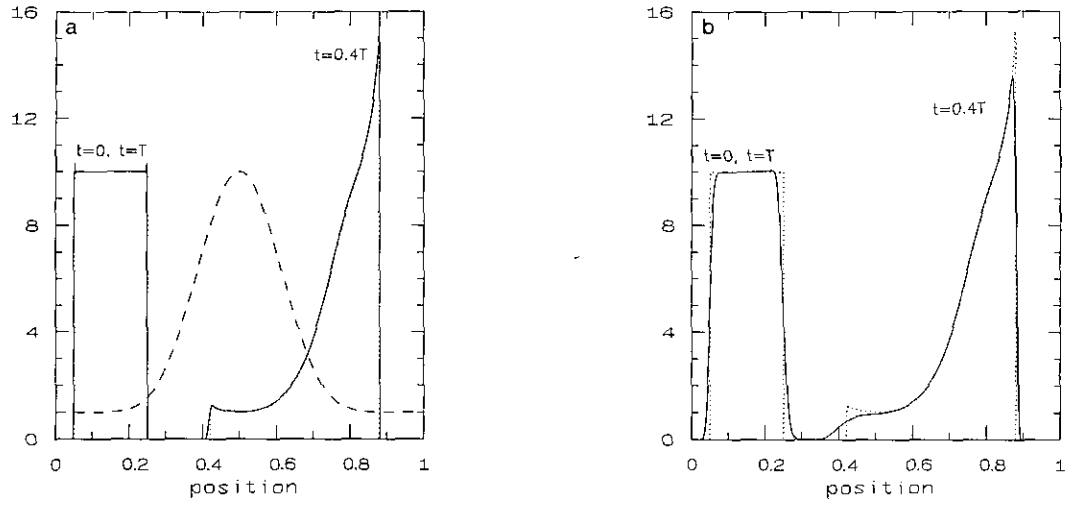

FIG. 4. (a) Time evolution ($t = 0$, $0.4T$, and T) of initial rectangular test function under influence of variable velocity (– – –): (· · ·), ideal solution; (———), finite element method solution. (b) Time evolution ($t = 0$, $0.4T$, and T) of initial rectangular test function under influence of variable velocity: (· · ·), ideal solution; (———), implicit finite difference method solution.

Gaussian wave) is then undertaken. Figures 5 show propagation of this Gaussian wave but without neglecting the diffusion as in Figs. 4. A constant drift velocity and diffusion coefficient values are chosen: $W_z = 10^6$ m/s, $D_z = 2 \times 10^3$ m^2/s for z varying in the range [0, 30 cm] and for $t_{max} = 2 \times 10^{-7}$ s. In Fig. 5a, finite element method results are given for a different number of discrete intervals, n_z and n_t, and Fig. 5b shows results obtained from an improved implicit · finite difference method using an exponential scheme [9]. As the number of discrete intervals n_z and n_t increases, finite element method results tend towards the optimum solution from the top and finite difference method results tend towards the same solution from the bottom. It is to be noted that both numerical schemes have a good convergency because the results tend towards an optimum solution (which is stable) as the mesh size decreases. These schemes also have good conservative property because the area of the initial density is well conserved during the time evolution of $n(z, t)$ in the present example chosen without a source term. However, a smaller number of discrete inter-

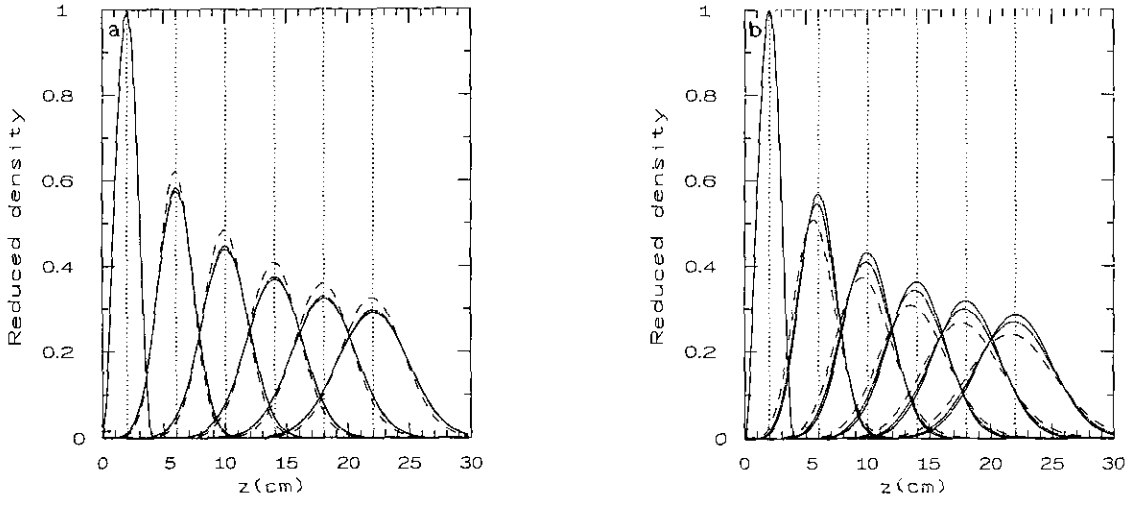

FIG. 5. (a) Time evolution ($t = 0$, 0.04, 0.08, 0.12, 0.16, and 0.2 μs) of an initial Gaussian test function for $W = 10^6$ m/s and $D = 2 \times 10^3$ m^2/s from the finite element method for different values of discretization intervals n_t and n_z: (– – –), $n_z = 100$, $n_t = 100$; (– · – ·), $n_z = 100$, $n_t = 200$; (———), $n_z = 100$, $n_t = 350$. (Vertical dotted lines correspond to the ideal position of the top of each wave for the different instants of the propagation.) (b) Time evolution ($t = 0$, 0.04, 0.08, 0.12, 0.16, and 0.2 μs) of an initial Gaussian test function for $W = 10^6$ m/s and $D = 2 \times 10^3$ m^2/s from the implicit finite difference method with exponential approximation for different values of discretization intervals n_t and n_z: (– – –), $n_z = 100$, $n_t = 100$; (– · – ·), $n_z = 500$, $n_t = 300$; (———), $n_z = 500$, $n_t = 3000$. (Vertical dotted lines correspond to the ideal position of the top of each wave for the different instants of the propagation.)

vals n_z and n_t (see legend of Fig. 5a) are necessary to reach the optimum solution in the case of the finite element method: the product of the discrete interval numbers $n_z \times n_t$ is lower by approximately a factor 40. In computing the time point of view, this means that the finite element method is faster by the same factor. Therefore, such a finite element method opens new perspectives for investigation and modeling of gas discharges, for example, for longer time scales, larger electrode separations, etc.

3.2. *Results in Real Discharges*

The following results are given to show the ability of the present work's numerical scheme to correctly treat the cases of real gas discharges dominated by space charge effects.

The first example chosen, already treated by Lowke and Davies [3], concerns a class of electrical gas discharges produced when a spatially uniform source (gamma rays created by fission fragments) continually ionizes the gas between two plane parallel metallic electrodes that is assumed, for calculations, to be perfectly absorbing and not emitting any particles. For certain values of gas pressure and applied potential, space charge effects—particularly in the sheath regions—become important in such discharges which behave as usual glow discharges. As in Lowke and Davies' work [3] the filling gas is Ar under 240 Torr pressure, 100 V applied voltage, and 3 mm gap length. For this gas pressure, the atomic Ar^+ ions initially produced by the uniform ionization source S_{ion} ($S_{ion} = 3.6 \times 10^{16}$ cm^{-3}/s) are rapidly converted, via three body reactions, into Ar_2^+ molecular ions. As conversion time is shorter than drift and diffusion times, it is quite correct to assume, following Lowke and Davies' explanation [3], that electrical behavior of the discharge is mainly governed by electrons and Ar_2^+ ions. This means that the space charge effect can be obtained from solution of the hydrodynamic equations of the electrons and the molecular Ar_2^+ ions produced either from Ar^+ generated by the uniform ionization source S_{ion} or from Ar^+ created by the impact on Ar atoms of electrons that are accelerated by the electric field. Furthermore, Ar_2^+ ions can vanish by electron–Ar_2^+ recombination processes with the coefficient α_{rec} ($\alpha_{rec} = 8.81 \times 10^{-7}$ cm^3/s). Therefore, the whole source term $S(z, t)$ of the hydrodynamic equations (4) for electrons and the Ar_2^+ ions to be solved can be written as

$$S(z, t) = S_{ion} + n_e(z, t)\, \nu_{ion} - \alpha_{rec} n_e(z, t)\, n_{Ar_2^+}(z, t). \quad (14)$$

It is to be noted that the transport coefficients for electrons and the Ar_2^+ ions (i.e., electron and ion drift velocity and longitudinal diffusion coefficients and also ionization frequency ν_{ion}) necessary for the solution of Eqs. (4) with source term (14) are taken from the literature [17].

Figure 6a shows transient and, also, steady state space variation of the electron and Ar_2^+ ion densities calculated from the finite element method solution of Eqs. (4) under the discharge conditions previously described, while Fig. 6b shows the variation of the calculated electric field and potential. Starting from the initial conditions (uniform electric field without space charge), the steady state results are reached under the influence of the permanent source uniform S_{ion} which sustains the discharge. These results show two distinct regions which behave as the classical cathodic sheath and negative glow of the usual glow discharge [18]. The well-pronounced cathodic sheath, in which the electric field rapidly decreases and the electron

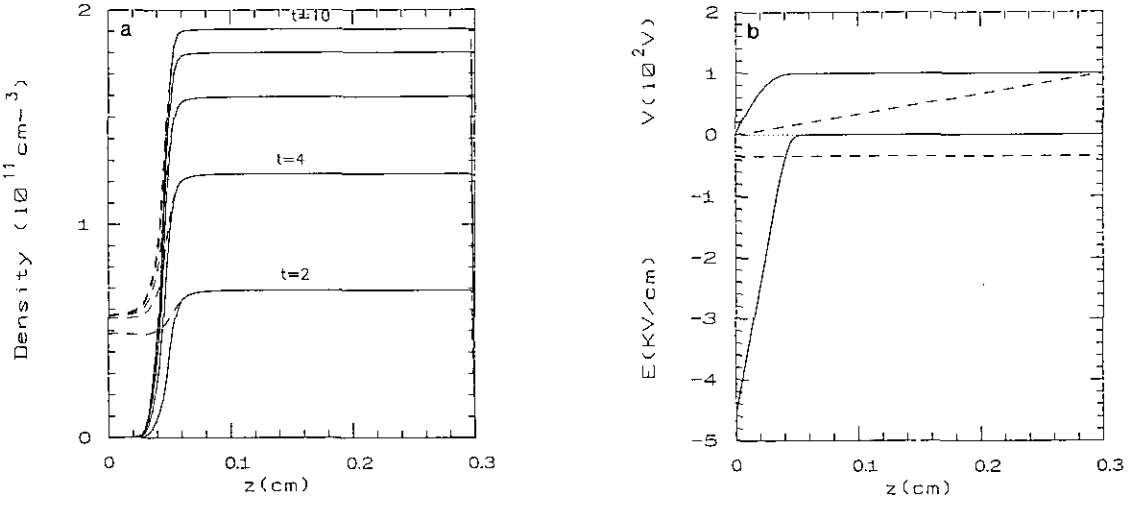

FIG. 6. (a) Time evolution ($t = 0$, 2, 4, 6, 8, and 10 μs) of electron (———) and Ar_2^+ ion (– – –) density in Ar discharge between two plane parallel electrodes for $V = 100$ V, $T_{gas} = 300$ K, $p_{Ar} = 240$ Torr, and permanent source $S_{ion} = 3.6 \times 10^{16}$ pair electron–ion cm^{-3}/s (i.e., under Lowke and Davies [3] conditions). (b) Initial (– – –) and steady state (———) electric field and potential in Ar discharge with $V = 100$ V, $T_{gas} = 300$ K, $p_{Ar} = 240$ Torr, and permanent source $S_{ion} = 3.6 \times 10^{16}$ pair electron–ion cm^{-3}/s (i.e., under Lowke and Davies [3] conditions).

density becomes quasi-negligible in comparison to the ion density, is due to the strong space charge effects existing in this region since the electron drift velocity is much higher than the ion drift velocity. The plasma region (or the negative glow region) is characterized by the electron and ion densities remaining constant and quasi-equal, leading to a practically negligible net charge so that the resulting electric field is negligible and the potential is constant. It is to be noted that the present results are in quite good agreement with Lowke and Davies's calculations [3].

The second example of the chosen real discharges concerns the propagation of ionizing waves in N_2 discharge between two plane parallel electrodes under overvoltage stress. The discharge conditions are not far from those of Dhali and Williams [7], i.e., 760 Torr gas pressure for 300 K background gas temperature, 5 mm gap separation, and 24 KV applied voltage (i.e., about 50% overvoltage). The discharge is initiated at the cathode by an initial neutral half Gaussian with peak height 10^{14} cm^{-3} and 1 mm radius. A uniform neutral background ionization density (one pair of electron–ion/cm^3) is also assumed. In fact, this uniform ionization background ensures the propagation of ionizing waves from cathode to anode without including photoionization processes in gas as in, for example, Yoshida and Tagashira's work [2]. It is to be noted that the aim of this paper is not to discuss the well-known question concerning the phenomena at the origin of the streamer propagation (gas photoionization or energetic electrons in the head streamer, or both, phenomena), but only to show the ability of the present numerical method to correctly treat the ionizing wave propagation problem under strong space charge effect. For this reason, the simplest case (i.e., a uniform ionization background) is chosen in the following calculations. Furthermore, the radial spread of the discharge cannot be assumed infinite as in the first example (glow discharge conditions). So, the Poisson equation needs to be solved either in 2D geometry (e.g., in Dhali and Williams or Kunhardt and Wu [7]) or in 1D geometry by using the image charge method proposed by Davies *et al.* [1]. The latter method (which is more appropriate to 1D Cartesian geometry) is used in this paper, assuming that the discharge is established uniformly in the radial direction inside a column with a constant radius ($R_c = 200\ \mu$m).

Figures 7a and b show space variation respectively of charged particle densities and electric field in N_2 discharge for different instants of evolution, under the discharge conditions previously described. The transport coefficients necessary for numerical solution of Eqs. (4) for electron and nitrogen ions are already given elsewhere [19]. In Figs. 7 most of the classical behaviors of anode directed ionizing waves are observed. Indeed, as time evolves from 0 to 2.1 ns, electron and ion densities move towards the anode since electrons of the initial density propagate towards the anode (ions are quasi-static in the present time scale, 0 to 2.1 ns) and simultaneously ionize the background gas, leading to positive ion formation. Therefore, the resulting net charge becomes progressively large, leading to a space charge effect which locally enhances the electric field (see Fig. 7b). Then, this high space charge electric field, showing a sharp gradient and justifying the name of "ionizing wave," accelerates seed electrons of uniform ionization background, thus producing new ionization in gases. This phenomenon, involving new strong space charge and a new corresponding sharp electric field, is repeated up to the anode. It is also noted that the results shown in Figs. 7 are in qualitatively good agreement with those of Dhali and Williams [7].

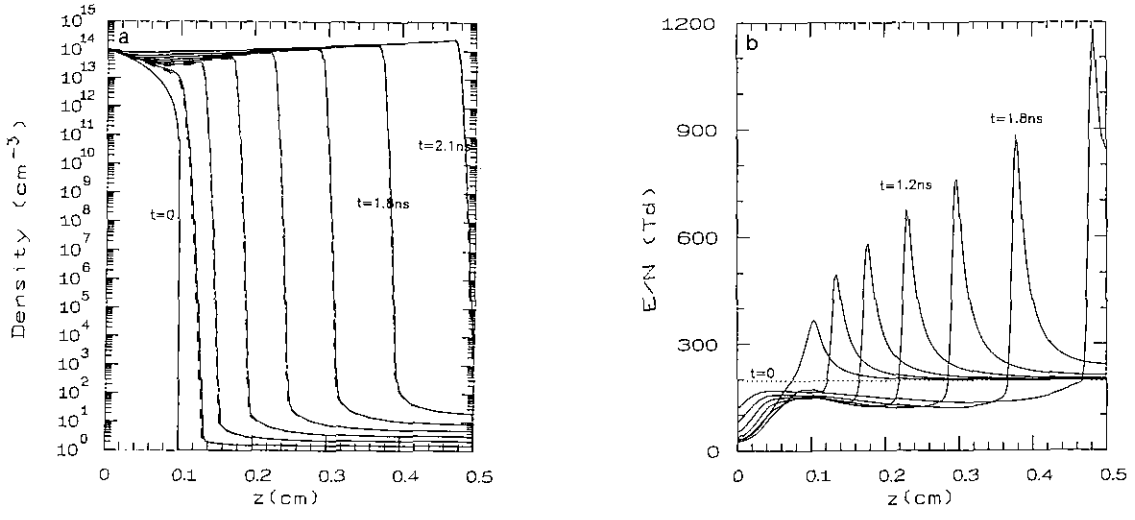

FIG. 7. (a) Time evolution ($t = 0$, 0.3, 0.6, 0.9, 1.2, 1.5, 1.8, and 2.1 ns) of electron (———) and ion (– – –) density in N_2 discharge between two plane parallel electrodes for $V = 24$ kV, $T_{gas} = 300$ K, and $p_{N_2} = 760$ Torr. (b) Initial (· · ·) and time evolution ($t = 0.3$, 0.6, 0.9, 1.2, 1.5, 1.8, and 2.1 ns) of electric field in N_2 discharge between two plane parallel electrodes for $V = 24$ kV, $T_{gas} = 300$ K, and $p_{N_2} = 760$ Torr.

4. CONCLUSION

In this paper, a specific finite element method is used, for the first time in the literature, for the solution of hydrodynamic conservation equations of charge carriers in the gas discharge area. The aim is simply to propose, for the reader, an additional method that presents different advantages from those of the usual finite difference methods, particularly in the case where there is discontinuity in the density variation. This numerical scheme is first checked, in the case of model discharges for the propagation of rectangular density, showing its ability to properly treat the difficult discontinuity problem. Then, by coupling Poisson equation to conservation equations of charge carriers, this numerical scheme is also successfully tested in the case of two real discharges characterized by dominant space charge effects: the cathodic region of an Ar glow discharge and propagation of ionizing waves in N_2 discharge under overvoltage and high pressure conditions. The next step is to extend this numerical method to the case of multidimensional geometry.

APPENDIX

Coefficients $\overline{z^l_{i+1/2}}$, $\zeta^{l+1}_{i+1/2}$, $\overline{\zeta^{l+1}_{i+1/2}}$, $\overline{t^m_{k+1/2}}$, $\tau^{m+1}_{k+1/2}$, and $\overline{\tau^{m+1}_{k+1/2}}$ which intervene in relations (11) and (12) are defined

$$\overline{z^l_{i+1/2}} = \int_{z_i}^{z_{i+1}} dz\, \frac{z^l}{\Delta z_{i+1/2}}; \qquad \zeta^{l+1}_{i+1/2} = \int_{z_i}^{z_{i+1}} dz\, z^l \frac{z - z_i}{\Delta z_{i+1/2}};$$

$$\overline{\zeta^{l+1}_{i+1/2}} = \int_{z_i}^{z_{i+1}} dz\, z^l \frac{z_{i+1} - z}{\Delta z_{i+1/2}}$$

$$\overline{t^m_{k+1/2}} = \int_{t_k}^{t_{k+1}} dt\, \frac{t^m}{\Delta t_{k+1/2}}; \qquad \tau^{m+1}_{k+1/2} = \int_{t_k}^{t_{k+1}} dt\, t^m \frac{t - t^k}{\Delta t_{k+1/2}};$$

$$\overline{\tau^{m+1}_{k+1/2}} = \int_{t_k}^{t_{k+1}} dt\, t^m \frac{t_{k+1} - t}{\Delta t_{k+1/2}}.$$

The system of four linear equations with four unknowns n_A, n_B, n_C, and n_D, obtained in each finite element $[z_i, z_{i+1}] \times [t_k, t_{k+1}]$ for the different values of l and m ($l = 0$ or 1 and $m = 0$ or 1), is given hereafter in the case of lighted sides AB and DC (shown in Fig. 2), i.e., in the case of particles moving forwards along the z axis (negative particles):

$$\begin{aligned}
&n_A \left\{ \overline{t^m_{k+1/2}}\,\overline{\zeta^{l+1}_{i+1/2}} - \overline{z^l_{i+1/2}}\,\tau^{m+1}_{k+1/2} \right.\\
&\quad \times \left(W_{z^{k+1/2}_{i+1/2}} - \frac{D_{z^{k+1/2}_{i+1}}}{\Delta z_{i+1/2}} - \frac{D_{z^{k+1/2}_i}}{\Delta z_{i-1/2}} \right)\\
&\quad \left. + z^l_i \tau^{m+1}_{k+1/2} \left(W_{z^{k+1/2}_i} - \frac{D_{z^{k+1/2}_i}}{\Delta z_i} \right) \right\}\\
&+ n_B \left\{ \left(-\overline{t^m_{k+1/2}} + t^m_k \right) \overline{\zeta^{l+1}_{i+1/2}} - \overline{z^l_{i+1/2}}\,\overline{\tau^{m+1}_{k+1/2}} \right.\\
&\quad \times \left(W_{z^{k+1/2}_{i+1/2}} - \frac{D_{z^{k+1/2}_{i+1}}}{\Delta z_{i+1/2}} - \frac{D_{z^{k+1/2}_i}}{\Delta z_{i-1/2}} \right)\\
&\quad \left. + z^l_i \overline{\tau^{m+1}_{k+1/2}} \left(W_{z^{k+1/2}_i} - \frac{D_{z^{k+1/2}_i}}{\Delta z_i} \right) \right\}\\
&+ n_C \left\{ \left(-\overline{t^m_{k+1/2}} + t^m_k \right) \zeta^{l+1}_{i+1/2} + \overline{z^l_{i+1/2}}\,\overline{\tau^{m+1}_{k+1/2}} \right.\\
&\quad \left. \times \left(W_{z^{k+1/2}_{i+1/2}} - \frac{D_{z^{k+1/2}_{i+1}}}{\Delta z_{i+1/2}} \right) \right\}\\
&+ n_D \left\{ \overline{t^m_{k+1/2}} \zeta^{l+1}_{i+1/2} + \overline{z^l_{i+1/2}} \tau^{m+1}_{k+1/2} \right.\\
&\quad \left. \times \left(W_{z^{k+1/2}_{i+1/2}} - \frac{D_{z^{k+1/2}_{i+1}}}{\Delta z_{i+1/2}} \right) \right\}\\
&= t^m_{k+1/2} z^l_{i+1/2} S(z_{i+1/2}, t_{k+1/2})\\
&\quad + t^m_k \overline{\zeta^{l+1}_{i+1/2}} n_{Bt} + t^m_k \zeta^{l+1}_{i+1/2} n_{Ct}\\
&\quad + z^l_i \overline{\tau^{m+1}_{k+1/2}} \left(W_{z^{k+1/2}_i} - \frac{D_{z^{k+1/2}_i}}{\Delta z_i} \right) n_{Bz}\\
&\quad + z^l_i \tau^{m+1}_{k+1/2} \left(W_{z^{k+1/2}_i} - \frac{D_{z^{k+1/2}_i}}{\Delta z_i} \right) n_{Az}\\
&\quad + \overline{z^l_{i+1/2}} \frac{D_{z^{k+1/2}_i}}{\Delta z_{i-1/2}} \left\{ \tau^{m+1}_{k+1/2} n(z_{i-1}, t_{k+1}) \right.\\
&\quad \left. + \overline{\tau^{m+1}_{k+1/2}} n(z_{i-1}, t_k) \right\}. \qquad \text{(A1)}
\end{aligned}$$

In the case of lighted sides CD and BC (shown in Fig. 2), i.e., in the case of particles moving backwards along the z axis (positive particles), Eq. (A1) becomes

$$\begin{aligned}
&n_A \left\{ \overline{t^m_{k+1/2}}\,\overline{\zeta^{l+1}_{i+1/2}} - \overline{z^l_{i+1/2}}\,\tau^{m+1}_{k+1/2} \right.\\
&\quad \left. \times \left(W_{z^{k+1/2}_{i+1/2}} + \frac{D_{z^{k+1/2}_i}}{\Delta z_{i+1/2}} \right) \right\}\\
&+ n_B \left\{ \left(-\overline{t^m_{k+1/2}} + t^m_k \right) \overline{\zeta^{l+1}_{i+1/2}} - \overline{z^l_{i+1/2}}\,\overline{\tau^{m+1}_{k+1/2}} \right.\\
&\quad \left. \times \left(W_{z^{k+1/2}_{i+1/2}} + \frac{D_{z^{k+1/2}_i}}{\Delta z_{i+1/2}} \right) \right\}\\
&+ n_C \left\{ \left(-\overline{t^m_{k+1/2}} + t^m_k \right) \zeta^{l+1}_{i+1/2} + \overline{z^l_{i+1/2}}\,\overline{\tau^{m+1}_{k+1/2}} \right.\\
&\quad \times \left(W_{z^{k+1/2}_{i+1/2}} + \frac{D_{z^{k+1/2}_{i+1}}}{\Delta z_{i+3/2}} + \frac{D_{z^{k+1/2}_i}}{\Delta z_{i+1/2}} \right)\\
&\quad \left. - z^l_{i+1} \overline{\tau^{m+1}_{k+1/2}} \left(W_{z^{k+1/2}_{i+1}} + \frac{D_{z^{k+1/2}_{i+1}}}{\Delta z_{i+1}} \right) \right\}
\end{aligned}$$

$$
\begin{aligned}
&+ n_D \left\{ \overline{t^m_{k+1/2} \zeta^{l+1}_{i+1/2}} + \overline{z^l_{i+1/2}} \tau^{m+1}_{k+1/2} \right. \\
&\times \left(W_{z^{k+1/2}_{i+1/2}} + \frac{D_{z^{k+1/2}_{i+1}}}{\Delta z_{i+3/2}} + \frac{D_{z^{k+1/2}_{i}}}{\Delta z_{i+1/2}} \right) \\
&\left. - z^l_{i+1} \tau^{m+1}_{k+1/2} \left(W_{z^{k+1/2}_{i+1}} + \frac{D_{z^{k+1/2}_{i+1}}}{\Delta z_{i+1}} \right) \right\} \\
&= t^m_{k+1/2} z^l_{i+1/2} S(z_{i+1/2}, t_{k+1/2}) \\
&+ t^m_k \overline{\zeta^{l+1}_{i+1/2}} n_{Bt} + t^m_k \zeta^{l+1}_{i+1/2} n_{Ct} \\
&- z^l_{i+1} \overline{\tau^{m+1}_{k+1/2}} \left(W_{z^{k+1/2}_{i+1}} + \frac{D_{z^{k+1/2}_{i+1}}}{\Delta z_{i+1}} \right) n_{Cz} \\
&- z^{l+1}_i \tau^{m+1}_{k+1/2} \left(W_{z^{k+1/2}_{i+1}} + \frac{D_{z^{k+1/2}_{i+1}}}{\Delta z_{i+1}} \right) n_{Dz} \\
&+ \overline{z^l_{i+1/2}} \frac{D_{z^{k+1/2}_{i+1}}}{\Delta z_{i+3/2}} \{ \tau^{m+1}_{k+1/2} n(z_{i+2}, t_{k+1}) \\
&+ \overline{\tau^{m+1}_{k+1/2}} n(z_{i+2}, t_k) \}. \qquad \text{(A2)}
\end{aligned}
$$

It is to be noted that in Eq. (A1), densities n_{Az}, n_{Bz}, n_{Ct}, $n(z_{i-1}, t_{k+1})$, and $n(z_{i-1}, t_{k+1})$ and in Eq. (A2), densities n_{Cz}, n_{Dz}, n_{Ct}, $n(z_{i+2}, t_{k+1})$, and $n(z_{i+2}, t_{k+1})$ appearing in the right-hand terms are already known, either from initial conditions and boundaries or from previous calculations undertaken in the surrounding grids.

Noting also that the drift velocity $W_z(z, t)$ is an algebraic quantity, this means that $W_z(z, t)$ is considered positive along the z axis (forwards direction) and negative for backwards direction.

REFERENCES

1. A. J. Davies, C. S. Davies, and C. J. Evans, *Proc. IEE* **118**, 816 (1971).
2. L. E. Kline, *J. Appl. Phys.* **45**, 2046 (1974); K. Yoshida and H. Tagashira, *J. Phys. D: Appl. Phys.* **9**, 491 (1976); I. Abbas and P. Bayle, *J. Phys D: Appl. Phys.* **13**, 1055 (1980).
3. J. J. Lowke and D. K. Davies, *J. Appl. Phys.* **48**, 4991 (1977).
4. R. Morrow, *J. Comput. Phys.* **43**, 1 (1981).
5. J. P. Boris and D. L. Book, *J. Comput. Phys.* **20**, 397 (1976).
6. S. T. Zalesak, *J. Comput. Phys.* **31**, 335 (1979).
7. S. K. Dhali and P. F. Williams, *Phys. Rev. A* **31**, 1219 (1985); *J. Appl. Phys.* **62**, 4696 (1987); R. Morrow, in *Proceedings, XVIII International Conference on Phenomena in Ionized Gases (Invited papers), University College of Swansea, 1987*, edited by W. T. Williams, p. 268; E. E. Kunhardt and C. Wu, *J. Comput. Phys.* **68**, 127 (1987).
8. D. L. Sharfetter and H. K. Gummel, *IEEE Trans. Electron. Devices* **ED-16**, 64 (1969).
9. J. P. Boeuf, *Phys. Rev. A* **36**, 2782 (1987); *J. Appl. Phys.* **63**, 1342 (1988).
10. A. Chatwiti and M. Yousfi, in *Proceedings, IX International Conference on Gas Discharges and their Applications, Venezia, 1988*, p. 383; A. Chatwiti, Thèse de Doctorat d'Etat n° 1381, Université Paul Sabatier, 1988.
11. E. E. Lewis, W. F. Miller, and T. P. Henry, *Nucl. Sci. Eng.* **58**, 203 (1975).
12. J..J. Barnes and R. J. Lomax, *IEEE Trans. Electron. Devices* **ED-24**, 1082 (1977).
13. Y. Chauvet, *Résolution de l'équation de transport instationnaire par des méthodes d'élements finis*, Internal report, CEA (Commissariat à l'energie Atomique) n° 2079, 1979 (unpublished).
14. P. Segur, M. Yousfi, J. P. Boeuf, E. Marode, A. J. Davies, and J. G. Evans, in *Electrical Breakdown and Gas Discharges. Part A. The Microscopic Treatment of Nonequilibrium Regions in a Weakly Ionized Gas*, edited by Kunhardt and Luessen (Plenum, New York, 1983), p. 331; A. J. Davies, *Proc. IEE* **133**, Pt. A, 217 (1986).
15. O. C. Zienkiewicz, *La méthode des éléments finis* (McGraw–Hill, Paris, 1971).
16. A. J. Davies, *Workshop on "Plasmas Chauds et Modélisation des Décharges," GDR SPARCH, Numerical Solutions of Continuity Equations and Plasma Growth, Marseille, 1992*, p. 45.
17. H. W. Ellis, R. Y. Pai, E. W. McDaniel, E. E. Mason, and L. A. Viehland, *At. Data Nucl. Tables* **17**, 177 (1976); H. W. Ellis, E. W. McDaniel, D. L. Albritton, L. A. Viehland, S. L. Lin, and E. E. Mason, *At. Data Nucl. Tables* **22**, 179 (1978); M. Yousfi, G. Zissis, A. Alkaa, and J. J. Damelincourt, *Phys. Rev. A* **42**, 978 (1990).
18. A. Von Engel, *Ionized Gases* (Oxford Univ. Press, Oxford, 1965).
19. M. Yousfi, A. Poinsignon, and A. Hamani, Electron data base needed for discharge modeling in flue gas treatment, in *Non-thermal Plasma Techniques for Pollution Control*, NATO ASI Series, Vol. G34A, edited by B. M. Penetrante and S. E. Schultheis (Springer-Verlag, Berlin/Heidelberg, 1993), p. 299.
20. A. Hennad, M. Yousfi, and A. Himoudi, in *Proceedings, XXI International Conference on Phenomena in Ionized Gases, Bochum, Germany, 1993*, Vol. II, p. 11.